Surface State Dissipation in Confined ^{3}He-*A*

Alexander J. Shook,* Emil Varga, Igor Boettcher, and John P. Davis†
Department of Physics, University of Alberta, Edmonton, Alberta T6G 2E9, Canada

(Received 16 September 2023; accepted 15 March 2024; published 9 April 2024)

We have studied the power dependence of superfluid Helmholtz resonators in flat (750 and 1800 nm) rectangular channels. In the *A* phase of superfluid ^{3}He, we observe a nonlinear response for velocities larger than a critical value. The small size of the channels stabilizes a static uniform texture that eliminates dissipative processes produced by changes in the texture. For such a static texture, the lowest velocity dissipative process is due to the pumping of surface bound states into the bulk liquid. We show that the temperature dependence of the critical velocity observed in our devices is consistent with this surface-state dissipation. Characterization of the force-velocity curves of our devices may provide a platform for studying the physics of exotic surface bound states in superfluid ^{3}He.

DOI: 10.1103/PhysRevLett.132.156001

One of the defining features of superfluidity is the ability to flow without dissipation for velocities below a critical value [1]. The Landau criterion states that this velocity threshold is set by a local minimum in the dispersion relation of the lowest energy excitation of the system [1]. For fermionic superfluids, the relevant energy scale is the superfluid gap, $\Delta_{\vec{p}}$, which is the energy required to excite a quasiparticle from the Fermi surface, and the Landau critical velocity is therefore $v_L = \Delta_{\vec{p}}/p_F$ [2].

Implicit in the arguments of Landau is the assumption that the gap is both spatially homogeneous and isotropic. In superfluid ^{3}He the latter assumption holds only for the bulk *B* phase, which has an isotropic gap. Near a surface, however, the gap is suppressed and develops separate parallel and perpendicular components [2,3]. The suppression of the gap near the wall breaks the Landau assumption and allows for bound states with energies less than the bulk gap. Experiments studying oscillating macroscopic objects in ^{3}He-*B* have shown that there is a sub-Landau critical velocity threshold at which bound states are emitted from a moving surface, leading to an observable change in dissipation [4,5]. Characterization of the coupling of these mechanical oscillators to fluid flow has proven to be a valuable tool for studying surface bound states in ^{3}He-*B* [4–10], which supplements other techniques [11–13]. These surface bound states are of interest not only from the perspective of understanding ^{3}He hydrodynamics [14] and quantum turbulence [15,16], but also as a condensed matter realization of exotic quasiparticles such as Weyl or Majorana fermions [17–26]. Experimental studies of surface bound state dissipation have thus far been limited to the *B* phase, as research on *A*-phase surface states is more complex due to the intrinsic anisotropy of the gap. Here, we reveal the pumping of surface bound states into the bulk *A* phase, with a lower critical velocity than the *B* phase due to additional suppressed states from the anisotropic *A*-phase gap.

In the *A* phase, there exists an anisotropy axis $\hat{\ell}$, which points in the direction of a Cooper pair's orbital angular momentum, along which the superfluid gap closes at two point nodes (see Fig. 1). Since the *A* phase exhibits long-range spatial ordering in the orbital angular momentum of Cooper pairs, $\hat{\ell}(\vec{r})$ is a vector field, or texture, which can vary smoothly in space over distances larger than the coherence length. The magnitude of the gap for a given

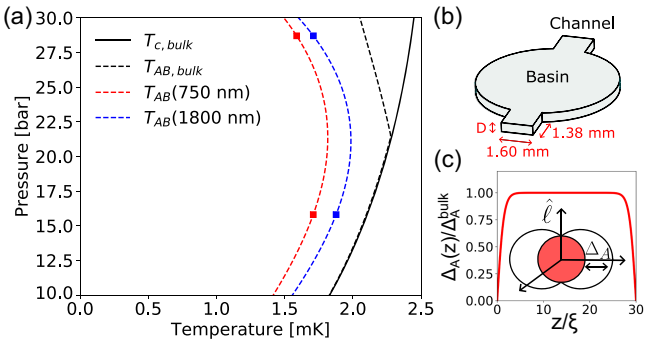

FIG. 1. *A*-phase flow. (a) Simplified phase diagram showing the range of temperatures where the *A* phase exists for 750 and 1800 nm channels. The red and blue points are the transition temperatures measured for both devices and the dashed lines are fits. The *A* phase is stabilized to lower temperatures and pressures by the tight confinement [27]. (b) Drawing of the confined Helmholtz resonator volume. The dimensions of the channel are $D \times 1.6$ mm $\times$ 1.38 mm, where $D = 750$ or 1800 nm. (c) Momentum space plot of the Fermi surface (red) and the gap which goes to zero at the poles aligned with the anisotropy vector $\hat{\ell}$. The plot shows the spatial dependence of $\Delta_A(z)$, in the highly confined dimension, where the distance from the wall is in units of the coherence length ξ. The spatial dependence has been computed using Ginzburg Landau theory [2].

momentum, $\vec{p}$, is specified by the equation $\Delta_{\vec{p}} = \Delta_A[1-(\hat{p}\cdot\hat{\ell})^2]^{1/2} = \Delta_A|\sin\theta|$. Here, θ is the angle between the momentum and anisotropy axis, such that the gap has a maximum magnitude, Δ_A, for excitations with momentum $\vec{p}\perp\hat{\ell}$ and a minimum magnitude of zero for $\vec{p}\|\hat{\ell}$. For this reason, naive application of the Landau criterion implies a critical velocity of zero.

Critical velocities of a different kind are possible in cases where the texture is dynamic. The motion of $\hat{\ell}$ changes the gap, and therefore dissipates energy by creating new excitations as it moves [28]. The texture couples both to superfluid phase gradients (i.e., flow), and to spin degrees of freedom [2]. In the absence of other orientational effects, the tendency of the $\hat{\ell}$ texture is to align with the superfluid flow velocity $\vec{v}_s$ [29]. This tendency is in competition with the boundary conditions, which requires the $\hat{\ell}$ texture to be perpendicular to surfaces. This means that ^{3}He-A flowing over a surface can produce a textural gradient where $\hat{\ell}$ is parallel to the flow far from the wall and perpendicular at the surface [29]. The characteristic length scale over which the texture rotates by 90° is the healing length, $\xi^A_{\mathrm{heal}} \sim 8$ μm [2]. For bulk systems, where all dimensions are large compared to the healing length, the texture becomes a hydrodynamic variable that exhibits complicated behavior, including critical velocities [30–35]. Systems where one or more dimensions are small compared to the textural healing length tend to lock a particular texture in place. This can be seen in the literature from experiments with varying degrees of confinement [36–46].

In cases where the texture is static, constant A-phase superfluid flow can be stable even when aligned with $\hat{\ell}$, because only a small number of states exist near the nodes. These states quickly fill when the fluid begins to flow, but once filled do not contribute to dissipation [47]. This produces a nonlinear relationship between the superfluid velocity and momentum density,

$$\vec{j}_s = \rho_s(v_s)\vec{v}_s. \tag{1}$$

The superfluid density, ρ_s, decreases with increasing velocity as excitations are produced. Thus the momentum density, $j_s(v_s)$, has a local maximum known as the maximum pair breaking current [2]. This relationship assumes the system is always near equilibrium such that the available states are filled. There is, therefore, no special velocity at which dissipation onsets for this static texture, constant flow, case.

Until now, an open question remained as to what critical velocities, if any, the A phase would exhibit if the texture is stationary but the flow is oscillatory. As with the dc flow case, excitations can be produced near the nodes for arbitrarily small velocities, but to continuously dissipate energy there must be some process by which these states are continuously populated, and then emptied. The most obvious candidate is the bound state pumping process already known to exist in the B phase [4,5].

Our experiment studies the critical dissipative behavior of the A phase using alternating flow in a parallel plate geometry with confinement much smaller than the healing length [27,48–51], ensuring a uniform texture. We have made use of our nanofluidic devices called Helmholtz resonators, which have been described in previous publications [27,52–54]. The devices are comprised of bonded quartz chips that have been etched to create a small volume sandwiched between the chips. The shape of this space is a circular basin (3.5 mm radius), with two 1.60×1.38 mm $\times$ D rectangular channels connecting it to the external helium bath. The variable D is the thickness of the enclosed space, which is constant throughout. The two devices used in this experiment had thicknesses of $D = 750 \pm 12$ and 1800 ± 12 nm.

Aluminum electrodes are patterned onto the quartz, creating a parallel plate capacitor inside the basin. The volume of the basin can be slightly decreased by an electrostatic force between the capacitor plates. When this plate motion is driven resonantly with the Helmholtz mode of the channels, fourth sound is driven. The normal fluid does not move in the channels because the viscous penetration depth, δ, is large compared to the confinement ($\delta \approx 400$ μm $\gg D$) [55]. Furthermore, the confinement is also small compared to the healing length ($D \ll \xi^A_{\mathrm{heal}} \approx 8$ μm) [2]. Therefore, the texture is uniformly aligned in the highly confined direction $\hat{z}$, effectively eliminating textural dissipation mechanisms.

The capacitance of the Helmholtz resonator varies in time when driven. The measured capacitance signal responds to changes in the basin fluid mass when the fourth sound resonance is driven. A model of this system, described in the Supplemental Material [56], relates the spatially averaged mass current, $\langle j_s\rangle$, to the measured detector voltage via the equation

$$\langle j_s\rangle = \frac{(1+2\Sigma)}{2C_0R_{\mathrm{trans}}}\left(\frac{\rho AD}{a}\right)\frac{V_{\mathrm{DET}}}{V_{\mathrm{dc}}}. \tag{2}$$

Here, C_0 is the undriven capacitance, R_{trans} is the current to voltage conversion factor of a transimpedance amplifier, ρ is the total mass density of the ^{3}He, V_{dc} is a bias voltage used to enhance the signal, A is the area of the basin, a is the cross-sectional area of the channel, and Σ is a small correction factor to account for the finite compressibility of the helium.

By performing repeated power-sweep measurements of the Helmholtz resonance, we can measure the drive dependence of the resonance amplitude [52]. As shown in Fig. 2, for low drives there is a linear regime where the peak amplitude is proportional to the drive voltage, suggesting that the superfluid density is independent of drive. Once the peak of the resonances crosses a critical value, V_c, there is a secondary regime where the amplitude

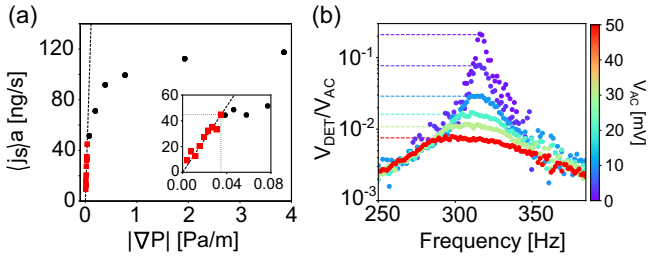

FIG. 2. Characterizing the nonlinear regime. (a) The mass current, calibrated from the detector peak voltage, for the 750 nm device at 22.45 bar and 2.08 mK is plotted as a function of the pressure gradient across the channels $|\nabla P|$. The bias voltage V_{dc} is held constant throughout the experiment such that $\langle j_s \rangle a \propto V_{\mathrm{DET}}$ and $|\nabla P| \propto V_{\mathrm{ac}}$. The inset highlights the linear drive regime and a critical value at which the slope abruptly changes. The dashed line is a fit to the linear regime data used to highlight the change in slope. The dotted lines indicate the point at which the slope changes. (b) Log-plot of the Helmholtz resonance with drive voltages ranging from 1 to 50 mV. The resonances are normalized by the drive voltage. Near resonance, the line shape distorts above the critical drive.

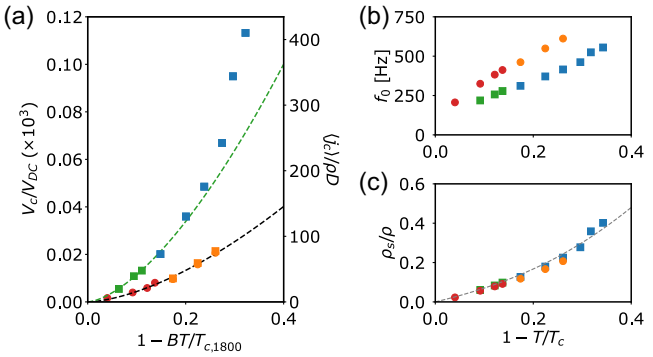

FIG. 3. Temperature scaling. (a) Plot of the peak voltage as a function of temperature for the 750 nm device at 22.45 bar (green squares), and 27.94 bar (blue squares), as well as 1800 nm device at 22.45 bar (red circles), and 27.94 bar (orange circles). The dashed lines show fits to functions of the form $(1 - BT/T_{c,1800})^{n/2}$. The parameter B is used to rescale the critical temperature for the 750 nm device. The 22.45 bar and 27.94 bar datasets are fit together for the 1800 nm device but separately for the 750 nm device. (b) Measured frequency dependence of the Helmholtz modes. (c) Superfluid density of each device as calculated from the resonant frequency. The gray curve is the bulk superfluid fraction.

increases at a slower rate and the line shape begins to flatten at the top of the resonance. The amplitude saturates for large drive voltages, suggesting that there is a maximum momentum density beyond which we cannot drive the resonator.

We characterize this effect by recording the detector voltage at which the slope changes for both devices at pressures of 2.87, 22.45, and 27.94 bar, over a range of temperatures. This voltage threshold was then converted into a critical current using Eq. (2). These results are compiled in Fig. 3. The temperature was determined using the known temperature dependence of the superfluid density [70], calibrated to a primary melting curve thermometer [71]. Specifically, the temperature of each data point was computed using the resonance frequency of the fourth sound mode of the 1800 nm device. The fourth sound mode frequency changes according to the equation

$$\left(\frac{\omega_0(T)}{\omega_0(0)}\right)^2 = \frac{\rho_s}{\rho}, \tag{3}$$

where $\omega_0(0)$ is a function of the resonator dimensions, total fluid density, and the isothermal compressibility. Inversion of this curve allows the measured frequency to be converted into a temperature as described in the Supplemental Material [53,56].

The temperature scaling was investigated by fitting 750 and 1800 nm amplitude datasets to a function of the form

$$\langle j_c \rangle = j_0(1 - BT/T_{c,1800})^{n/2}. \tag{4}$$

The prefactor B is included to account for the suppression of the critical temperature due to confinement. For the 1800 nm device $B = 1$, and for the 750 nm device it is the ratio of the two critical temperatures $B = T_{c,1800}/T_{c,750} = 1.042$. The value of this ratio is inferred by measuring the mode frequency as a function of temperature and extrapolating to zero frequency.

For the 1800 nm device, both pressure datasets are well fit by $n = 3.20$. For the 750 nm device, a similar curve, $n = 3.13$, can be fit to the data, but it deviates from this trend at lower temperatures. The fact that the A phase persists to lower temperatures under higher confinement allows us to measure a wider range of temperatures in the 750 nm device. The deviation from a $3/2$ power law appears to be a consequence of the fact that the superfluid fraction is approximately linear near T_c, but not at lower temperatures.

The critical currents are converted into critical velocities, by taking the ratio $v_c = \langle j_c \rangle / \rho_{s,c}$. Here, $\rho_{s,c} = \rho_s(v_c)$ is the velocity-dependent superfluid density computed from the measured Helmholtz frequency at the critical value. We find the critical velocity curves for the two devices, at three different pressures, come close to falling onto one another (see Fig. 4) and are not inconsistent with a function of the form

$$v_c = v_0(1 - BT/T_{c,1800})^{1/2}, \tag{5}$$

which is the same temperature scaling as the Ginzburg-Landau gap. The temperature-independent prefactor of the fit is $v_0 = 2.65 \pm 0.09$ mm/s. This is reminiscent of the Landau critical velocity for an isotropic superfluid

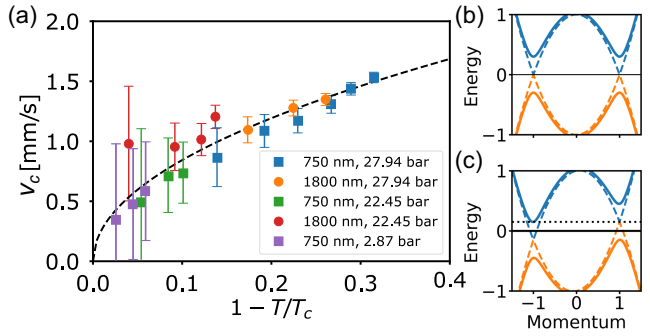

FIG. 4. Critical velocity. (a) The critical current of the Helmholtz resonator is computed from the resonance amplitude at which the linear regime ends, and the superfluid density from the center frequency of the resonance as $v_c = \langle j_s \rangle / \rho_{s,c}$. The ratio of these values is the critical velocity. The dashed line is a fit to all datasets of the form $v_0\sqrt{1 - T/T_c}$. (b) Plot of the quasiparticle dispersion relation when the fluid is at rest. The solid lines represent the bulk dispersion relation, and the dashed lines the bound state dispersion. (c) Plot of the quasiparticle dispersion relation at a finite critical velocity when the maximum energy value of the lower-band bound states is equal to the minimum energy value of the upper-band bulk states (highlighted by the dotted line).

$v_L(T) = \Delta(T)/p_F$. However, the analogy is not straightforward due to the existence of the A-phase nodes.

Comparing our results to the dc flow experiments performed by Manninen *et al.* [44,45], which studied flow through an 0.8 μm Nuclepore filter, multiple dissipation regimes were observed only in cases where the end effects produced orbital viscosity. These end effects occurred only when the A phase existed both inside and outside the pores, but not when the superfluid was B phase outside the pores and A phase inside. In light of this, it is worth considering the phase transitions of the bulk fluid outside the Helmholtz resonator. At 22.45 bar the bulk A to B transition occurs at $T_{AB} = 0.979T_c$, redat 27.94 bar it is $T_{AB} = 0.876T_c$, and at 2.87 bar it does not occur at all. This means that in the majority of our measurements the fluid outside the Helmholtz resonator is B phase. To study the role of the boundary, we performed a measurement at 27.94 bar at 2.37 mK, which is above the bulk T_{AB} line, ensuring A phase both inside and outside the Helmholtz resonator. We found the critical velocity follows the same temperature scaling, suggesting the phase boundary plays no role [56]. In the experiments of Ref. [44,45] where the A-phase texture was static, there was no special velocity at which dissipation onsets, as expected for dc flow. This suggests that the dissipation onset velocity we observe is unique to the dynamics of oscillatory flow resulting from our ac Helmholtz resonance.

To understand the role of oscillatory flow, we now consider in more detail the mechanical oscillator experiments performed in ^{3}He-B [4,5]. Near the surface of a moving object, the gap is suppressed allowing for bound state excitations localized near the surface. Similar to the states near the A-phase nodes, these states do not contribute to dissipation once filled, unless they can escape into the bulk fluid. When the flow is alternating, with an oscillation period that is large compared to the quasiparticle lifetime, a pumping process can occur at a fraction of the Landau critical velocity when the energy of a bound state exceeds that of an unoccupied bulk state. This allows for dissipation as the surface states are continuously populated and released. There does not seem to be any conceptual reason why this same process should not occur in the A phase and, when textural dynamics are eliminated, we argue it should be the lowest energy critical velocity. Since the critical velocity due to bound state dissipation is proportional to the gap magnitude, this is consistent with the temperature scaling we observe. It is worth mentioning that although the previously mentioned mechanical oscillator experiments [4,5] needed to cool to the ballistic temperature regime to study bound state dissipation, this is due primarily to the normal fluid viscosity. Since our experiment is based on a superleak, a critical velocity due to bound states could in principle be measured at any temperature, though the existence of thermal excitations may modify the results quantitatively (see discussion in Supplemental Material [56]).

We note that the flow inside the Helmholtz resonator is quite different from a vibrating wire. Because of viscous clamping of the normal fluid, there is no analogous backflow parameter for the Helmholtz resonator. Analysis of the flow fields, however, shows that there is localized flow enhancement at the corners of the channels. Our simulations (discussed in the Supplementary Material [56]) suggest that the peak flow velocity at the corners may be a factor of ∼10 times larger than the spatially averaged channel velocity that we calculate from our measurements. For this reason, bound state dissipation is likely initially localized to a region near the corners. Our experiment is only sensitive to the average velocity, therefore the values we report in Fig. 4(a) may not reflect the velocity at pair breaking [72]. Future experiments will investigate the effects of rounded corners on the critical velocity. Such rounded corners will ensure uniform velocity, hence quantitative measurements of the pair-breaking velocity.

We argue in the Supplemental Material that the confinement does not permit textural transitions even when the flow enhancement is considered [56]. The question of dissipation due to vortices (i.e., nucleation at the channel corners, or a vortex mill process) is also explored in the Supplemental Material [56], which has been considered as an alternative interpretation of the observed critical velocity. We offer several arguments against this view, the most important of which is the difference in the nonlinear scaling we observe in the B phase compared to the A phase. Any dissipative process involving pure phase winding vortices, which exist in both the A and B phases, should give rise to a similar critical velocity in both phases. Contrary to this, we

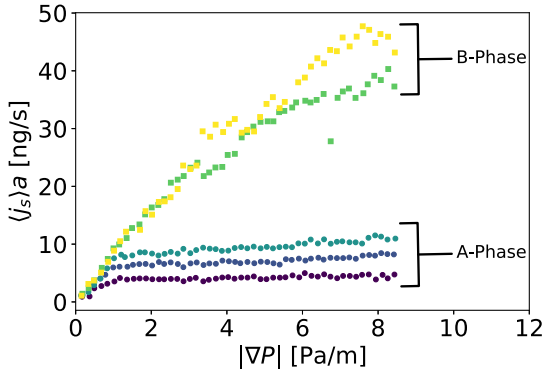

FIG. 5. Plot of the resonance peak height as a function of drive voltage, measured for the 1800 nm device at 28 bar for a variety of temperatures near the A-B critical temperature. The A-phase data are plotted in circles, and the B phase in squares. Lower temperature measurements have higher amplitudes due to the increased superfluid fraction. For low drives, the drive-amplitude relationship is linear for both A and B phases. Above the A-phase critical velocity, the trend deviates for the A phase as the line shape becomes distorted with a flat top, whereas in the B phase this flattening does not occur.

find a drastically different drive scaling for the B phase. Figure 5 shows how the peak height of the Helmholtz resonance scales with the drive voltage for the 1800 nm device at 27.94 bar, for temperatures above and below the A-B transition temperature. In the A phase there is an obvious critical drive where the slope changes as the resonance line shape begins to distort. For the B phase the scaling remains linear for higher drives, eventually displaying a qualitatively different type of nonlinearity. Instead of the resonance line shape becoming flatter, it develops a bistability, which will be explored elsewhere.

The fact that the B phase does not display the same critical velocity as the A phase suggests that the dissipation mechanism must either be unique to the A phase or simply occur at higher velocities in the B phase. A simple model has been constructed in the Supplemental Material to explain this difference [56]. This model suggests that the existence of bulk states near the A-phase nodes modifies the critical velocity, compared to an isotropic superfluid, by a factor of $\sin(\theta_{\max}) \approx 0.57$–$0.85$ depending on pressure. Since the A-phase gap is proportional to $\sin(\theta)$, the low energy states near the node preferentially fill up first. The value $\theta_{\max}$ is introduced as an effective quantity that sets the minimum energy of available bulk states for surface states to scatter into. The combination of this correction factor, and the corner flow enhancement, accounts for the relatively low critical velocity measured in our experiment.

In conclusion, we have carried out measurements of the force-velocity curves for oscillatory flow in ^{3}He-A in channels with thicknesses of 1800 and 750 nm. We find dissipation onsets at a critical velocity that has the same temperature scaling as the Ginzburg-Landau gap. This critical velocity is best explained by the pumping of surface bound states in our devices, an effect that has not previously been shown in ^{3}He-A. Our experiment studies channel sizes that are still large compared to the gap suppressed region where bound states are localized. In this regime, our measurement of the critical velocity does not show any notable dependence on the channel height or pressure.

In future experiments, we are interested in investigating the confinement limit where the channel thickness is comparable to—or even smaller than—the coherence length, a regime that is beginning to be experimentally accessible, such as in NMR devices of 192 nm [73] and Helmholtz resonators as small as 25 nm [74]. Theoretical work suggests that the A phase is favored over the planar phase even in this highly confined limit when strong coupling is considered [48,50]. In this highly confined regime, the gap suppression should extend across the entire channel, which we expect to have consequences for the critical velocity. Using the pressure and temperature dependence of the coherence length, $\xi(P,T)$, gives us an *in situ* knob to change the ratio D/ξ. Studying the Helmholtz mode force-velocity curves as a function of this ratio is thus a platform for probing the properties of bound states in both ^{3}He-A and ^{3}He-B, which are predicted to be exotic Weyl [19,22,23,26] and Majorana quasiparticles [75,76].

The authors acknowledge that the land on which this work was performed is in Treaty Six Territory, the traditional territories of many First Nations, Métis, and Inuit in Alberta. They acknowledge fruitful discussions with C. Sun and F. Marsiglio, as well as support from the University of Alberta and the Natural Sciences and Engineering Research Council, Canada (Grants No. RGPIN-2022-03078, No. CREATE-495446-17, No. RGPIN-2021-02534, and No. DGECR2021-00043).

*ashook@ualberta.ca
†jdavis@ualberta.ca

[1] I. M. Khalatnikov, *An Introduction to the Theory of Superfluidity* (CRC Press, Boca Raton, 2018).
[2] D. Vollhardt and P. Wolfle, *The Superfluid Phases of Helium-3* (Courier Corporation, Chelmsford, 2013).
[3] M. J. Rudd, P. S. Yapa, A. J. Shook, J. Maciejko, and J. P. Davis, Strong-coupling corrections to hard domain walls in superfluid ^{3}He-B, Phys. Rev. B **104**, 094520 (2021).
[4] C. A. M. Castelijns, K. F. Coates, A. M. Guénault, S. G. Mussett, and G. R. Pickett, Landau critical velocity for a macroscopic object moving in superfluid ^{3}He-B: Evidence for gap suppression at a moving surface, Phys. Rev. Lett. **56**, 69 (1986).
[5] D. I. Bradley, S. N. Fisher, A. M. Guénault, R. P. Haley, C. Lawson, G. R. Pickett, R. Schanen, M. Skyba, V. Tsepelin, and D. Zmeev, Breaking the superfluid speed limit in a fermionic condensate, Nat. Phys. **12**, 1017 (2016).

[6] M. Skyba and P. Skyba, High quality tuning forks in superfluid ^{3}He-B below 200 μK, J. Low Temp. Phys. **162**, 669 (2011).
[7] P. Zheng, W. G. Jiang, C. S. Barquist, Y. Lee, and H. B. Chan, Critical velocity in the presence of surface bound states in superfluid ^{3}He-B, Phys. Rev. Lett. **118**, 065301 (2017).
[8] M. T. Noble, S. L. Ahlstrom, D. I. Bradley, E. A. Guise, R. P. Haley, S. Kafanov, G. R. Pickett, M. Poole, R. Schanen, T. Wilcox, A. J. Woods, D. E. Zmeev, V. Tsepelin *et al.*, Producing and imaging quantum turbulence via pair-breaking in superfluid ^{3}He-B, Phys. Rev. B **105**, 174515 (2022).
[9] S. Autti, R. Haley, A. Jennings, G. Pickett, M. Poole, R. Schanen, A. Soldatov, V. Tsepelin, J. Vonka, V. Zavjalov *et al.*, Quasiparticle transport in a two-dimensional boundary superfluid, Nat. Commun. **14**, 6819 (2023).
[10] S. Autti, S. Ahlstrom, R. Haley, A. Jennings, G. Pickett, M. Poole, R. Schanen, A. Soldatov, V. Tsepelin, J. Vonka *et al.*, Fundamental dissipation due to bound fermions in the zero-temperature limit, Nat. Commun. **11**, 4742 (2020).
[11] J. Scott, M. Nguyen, D. Park, and W. Halperin, Magnetic susceptibility of andreev bound states in superfluid ^{3}He-B, Phys. Rev. Lett. **131**, 046001 (2023).
[12] D. Lotnyk, A. Eyal, N. Zhelev, T. Abhilash, E. Smith, M. Terilli, J. Wilson, E. Mueller, D. Einzel, J. Saunders *et al.*, Thermal transport of helium-3 in a strongly confining channel, Nat. Commun. **11**, 4843 (2020).
[13] S. Autti, J. T. Mäkinen, J. Rysti, G. E. Volovik, V. V. Zavjalov, and V. B. Eltsov, Exceeding the Landau speed limit with topological Bogoliubov Fermi surfaces, Phys. Rev. Res. **2**, 033013 (2020).
[14] J. A. Kuorelahti, S. M. Laine, and E. V. Thuneberg, Models for supercritical motion in a superfluid Fermi liquid, Phys. Rev. B **98**, 144512 (2018).
[15] S. N. Fisher, M. J. Jackson, Y. A. Sergeev, and V. Tsepelin, Andreev reflection, a tool to investigate vortex dynamics and quantum turbulence in ^{3}He-B, Proc. Natl. Acad. Sci. U.S.A. **111**, 4659 (2014).
[16] V. Tsepelin, A. W. Baggaley, Y. A. Sergeev, C. F. Barenghi, S. N. Fisher, G. R. Pickett, M. J. Jackson, and N. Suramlishvili, Visualization of quantum turbulence in superfluid ^{3}He-B: Combined numerical and experimental study of Andreev reflection, Phys. Rev. B **96**, 054510 (2017).
[17] S. B. Chung and S.-C. Zhang, Detecting the Majorana fermion surface state of ^{3}He-B through spin relaxation, Phys. Rev. Lett. **103**, 235301 (2009).
[18] Y. Tsutsumi, T. Mizushima, M. Ichioka, and K. Machida, Majorana edge modes of superfluid ^{3}He A-phase in a slab, J. Phys. Soc. Jpn. **79**, 113601 (2010).
[19] M. A. Silaev and G. E. Volovik, Topological Fermi arcs in superfluid ^{3}He, Phys. Rev. B **86**, 214511 (2012).
[20] H. Ikegami, Y. Tsutsumi, and K. Kono, Chiral symmetry breaking in superfluid ^{3}He-A, Science **341**, 59 (2013).
[21] Y. J. Park, S. B. Chung, and J. Maciejko, Surface majorana fermions and bulk collective modes in superfluid ^{3}He-B, Phys. Rev. B **91**, 054507 (2015).
[22] O. Shevtsov and J. A. Sauls, Electron bubbles and Weyl fermions in chiral superfluid ^{3}He-A, Phys. Rev. B **94**, 064511 (2016).
[23] G. E. Volovik, On the chiral magnetic effect in Weyl superfluid ^{3}He-A, JETP Lett. **105**, 34 (2017).
[24] A. B. Vorontsov, Andreev bound states in superconducting films and confined superfluid ^{3}He, Phil. Trans. R. Soc. A **376**, 20150144 (2018).
[25] H. S. Byun, J. Jeong, K. Kim, S. G. Kim, S. B. Shim, J. Suh, and H. Choi, Measuring angular momentum of $p_x + ip_y$ topological superfluids: A proposal, Phys. Rev. B **98**, 024518 (2018).
[26] H. Wu and J. Sauls, Weyl fermions and broken symmetry phases of laterally confined ^{3}He films, J. Phys. Condens. Matter **35**, 495402 (2023).
[27] A. J. Shook, V. Vadakkumbatt, P. Senarath Yapa, C. Doolin, R. Boyack, P. H. Kim, G. G. Popowich, F. Souris, H. Christani, J. Maciejko, and J. P. Davis, Stabilized pair density wave via nanoscale confinement of superfluid ^{3}He, Phys. Rev. Lett. **124**, 015301 (2020).
[28] M. Cross, Orbital dynamics of the Anderson-Brinkman-morel phase of superfluid ^{3}He, J. Low Temp. Phys. **26**, 165 (1977).
[29] P. De Gennes and D. Rainer, Alignment of anisotropic superfluids by flow, Phys. Lett. **46A**, 429 (1974).
[30] G. Volovik and V. Mineev, Hydrodynamics of the A phase of superfluid ^{3}He, JETP Lett. **24**, 561 (1976), http://jetp.ras.ru/cgi-bin/e/index/e/44/3/p591?a=list.
[31] N. Mermin and T.-L. Ho, Circulation and angular momentum in the a phase of superfluid helium-3, Phys. Rev. Lett. **36**, 594 (1976).
[32] P. Bhattacharyya, T. L. Ho, and N. D. Mermin, Stability of superflow in ^{3}He-A, Phys. Rev. Lett. **39**, 1290 (1977).
[33] M. Cross and M. Liu, Stability of the aligned state of ^{3}He-A in a superflow, J. Phys. C **11**, 1795 (1978).
[34] A. L. Fetter, Hydrodynamic stability of ^{3}He-A, Phys. Rev. Lett. **40**, 1656 (1978).
[35] H. Kleinert, The two superflows in ^{3}He-A, Phys. Lett. **71A**, 66 (1979).
[36] R. Johnson, R. Kleinberg, R. Webb, and J. Wheatley, Heat flow in superfluid ^{3}He, J. Low Temp. Phys. **18**, 501 (1975).
[37] M. Bagley, P. Main, J. Hook, D. Sandiford, and H. Hall, Direct observation of orbital dissipation and superflow collapse in ^{3}He-A, J. Phys. C **11**, L729 (1978).
[38] J. M. Parpia and J. D. Reppy, Critical velocities in superfluid ^{3}He, Phys. Rev. Lett. **43**, 1332 (1979).
[39] A. J. Dahm, D. S. Betts, D. F. Brewer, J. Hutchins, S. J. Saunders, and W. S. Truscott, Dissipation in the flow of ^{3}He-A and ^{3}He-B through a narrow rectangular channel, Phys. Rev. Lett. **45**, 1411 (1980).
[40] M. A. Paalanen and D. D. Osheroff, Dissipation of flow in superfluid ^{3}He-A, Phys. Rev. Lett. **45**, 362 (1980).
[41] V. Kotsubo, K. D. Hahn, and J. M. Parpia, Suppression of superfluidity of ^{3}He in cylindrical channels, Phys. Rev. Lett. **58**, 804 (1987).
[42] J. Kasai, Y. Okamoto, K. Nishioka, T. Takagi, and Y. Sasaki, Chiral domain structure in superfluid ^{3}He-A studied by magnetic resonance imaging, Phys. Rev. Lett. **120**, 205301 (2018).
[43] J. Daunt, R. Harris-Lowe, J. Harrison, A. Sachrajda, S. Steel, R. Turkington, and P. Zawadski, Critical temperature

and critical current of thin-film superfluid ^{3}He, J. Low Temp. Phys. **70**, 547 (1988).
[44] M. T. Manninen, J. P. Pekola, R. G. Sharma, and M. S. Tagirov, Critical current of ^{3}He-A in narrow channels, Phys. Rev. B **26**, 5233 (1982).
[45] M. Manninen and J. Pekola, Flow of superfluid ^{3}He through micrometer-size channels, J. Low Temp. Phys. **52**, 497 (1983).
[46] E. Thuneberg and J. Kurkijärvi, Difficulties of supercurrents in narrow pores of ^{3}He-A, Phys. Lett. **86A**, 35 (1981).
[47] G. E. Volovik, Superfluid properties of ^{3}He-A, Sov. Phys. Usp. **27**, 363 (1984).
[48] P. S. Yapa, R. Boyack, and J. Maciejko, Triangular pair density wave in confined superfluid ^{3}He, Phys. Rev. Lett. **128**, 015301 (2022).
[49] N. Zhelev, T. S. Abhilash, E. Smith, R. Bennett, X. Rojas, L. Levitin, J. Saunders, and J. Parpia, The A-B transition in superfluid helium-3 under confinement in a thin slab geometry, Nat. Commun. **8**, 15963 (2017).
[50] C. Sun, A. Attar, and I. Boettcher, Superfluid phase transition of nanoscale-confined helium-3, Phys. Rev. B **108**, 144503 (2023).
[51] L. V. Levitin, B. Yager, L. Sumner, B. Cowan, A. J. Casey, J. Saunders, N. Zhelev, R. G. Bennett, and J. M. Parpia, Evidence for a spatially modulated superfluid phase of ^{3}He under confinement, Phys. Rev. Lett. **122**, 085301 (2019).
[52] E. Varga, V. Vadakkumbatt, A. J. Shook, P. H. Kim, and J. P. Davis, Observation of bistable turbulence in quasi-two-dimensional superflow, Phys. Rev. Lett. **125**, 025301 (2020).
[53] X. Rojas and J. P. Davis, Superfluid nanomechanical resonator for quantum nanofluidics, Phys. Rev. B **91**, 024503 (2015).
[54] E. Varga and J. P. Davis, Electromechanical feedback control of nanoscale superflow, New J. Phys. **23**, 113041 (2021).
[55] J. Reppy, Superfluid density and viscosity measurements in liquid ^{3}He, Physica (Amsterdam) **90B+C**, 64 (1977).
[56] See Supplemental Material at http://link.aps.org/supplemental/10.1103/PhysRevLett.132.156001, which includes Refs. [57–69] for discussion of the data calibration, calculations regarding alternative dissipation mechanisms, simulation of the corner flow, and a simple mathematical model of the critical velocity due to surface excitations.
[57] K. Ichikawa, S. Yamasaki, H. Akimoto, T. Kodama, T. Shigi, and H. Kojima, Healing length of superfluid ^{3}He, Phys. Rev. Lett. **58**, 1949 (1987).
[58] M. R. Freeman and R. C. Richardson, Size effects in superfluid ^{3}He films, Phys. Rev. B **41**, 11011 (1990).
[59] L. D. Landau and E. M. Lifshitz, *Fluid Mechanics: Landau and Lifshitz: Course of Theoretical Physics, Volume 6* (Elsevier, New York, 2013), Vol. 6.
[60] A. B. Vorontsov and J. A. Sauls, Thermodynamic properties of thin films of superfluid ^{3}He-A, Phys. Rev. B **68**, 064508 (2003).
[61] D. S. Buchanan, G. W. Swift, and J. C. Wheatley, Velocity of propagation of the ^{3}He A-B interface in hypercooled ^{3}He-A, Phys. Rev. Lett. **57**, 341 (1986).
[62] M. Bartkowiak, S. N. Fisher, A. Guénault, R. P. Haley, G. R. Pickett, M. Rogge, and P. Skyba, The unique superfluid ^{3}He AB interface: Surface tension and contact angle, J. Low Temp. Phys. **126**, 533 (2002).
[63] V. Fréedericksz and V. Zolina, Forces causing the orientation of an anisotropic liquid, Trans. Faraday Soc. **29**, 919 (1933).
[64] W. H. Zurek, Cosmological experiments in superfluid helium?, Nature (London) **317**, 505 (1985).
[65] V. Ruutu, Ü. Parts, J. Koivuniemi, N. Kopnin, and M. Krusius, Intrinsic and extrinsic mechanisms of vortex formation in superfluid ^{3}He-B, J. Low Temp. Phys. **107**, 93 (1997).
[66] K. W. Schwarz, Phase slip and turbulence in superfluid ^{4}He: A vortex mill that works, Phys. Rev. Lett. **64**, 1130 (1990).
[67] C. F. Barenghi, R. J. Donnelly, and W. Vinen, *Quantized Vortex Dynamics and Superfluid Turbulence* (Springer Science & Business Media, New York, 2001), Vol. 571.
[68] D. I. Bradley, S. N. Fisher, A. Guénault, R. P. Haley, M. Holmes, S. O'Sullivan, G. R. Pickett, and V. Tsepelin, Grid turbulence in superfluid ^{3}He-B at low temperatures, J. Low Temp. Phys. **150**, 364 (2008).
[69] P. M. Walmsley, I. J. White, and A. I. Golov, Intrinsic pinning of vorticity by domain walls of l texture in superfluid ^{3}He-A, Phys. Rev. Lett. **93**, 195301 (2004).
[70] J. Parpia, D. Wildes, J. Saunders, E. Zeise, J. Reppy, and R. Richardson, The temperature and pressure dependence of the normal fraction of superfluid ^{3}He-B, J. Low Temp. Phys. **61**, 337 (1985).
[71] D. S. Greywall and P. A. Busch, ^{3}He-melting-curve thermometry, J. Low Temp. Phys. **46**, 451 (1982).
[72] C. Lambert, Theory of pair breaking by vibrating macroscopic objects in superfluid ^{3}He, Physica (Amsterdam) **178B**, 294 (1992).
[73] P. Heikkinen, A. Casey, L. Levitin, X. Rojas, A. Vorontsov, P. Sharma, N. Zhelev, J. Parpia, and J. Saunders, Fragility of surface states in topological superfluid ^{3}He, Nat. Commun. **12**, 1574 (2021).
[74] E. Varga, C. Undershute, and J. P. Davis, Surface-dominated finite-size effects in nanoconfined superfluid helium, Phys. Rev. Lett. **129**, 145301 (2022).
[75] Y. Tsutsumi and K. Machida, Edge current due to majorana fermions in superfluid ^{3}He-A and B-phases, J. Phys. Soc. Jpn. **81**, 074607 (2012).
[76] H. Wu and J. A. Sauls, Majorana excitations, spin and mass currents on the surface of topological superfluid ^{3}He-B, Phys. Rev. B **88**, 184506 (2013).